Ground-to-UAV Communication Network: Stochastic Geometry-based Performance Analysis

Yalin Liu*, Hong-Ning Dai*, Muhammad Imran†, Nidal Nasser‡
*Macau University of Science and Technology, Macau SAR,
yalin_liu@foxmail.com; hndai@ieee.org
†King Saud University, Saudi Arabia,
dr.m.imran@ieee.org
‡College of Engineering, Alfaisal University, Saudi Arabia,
nnidal@gmail.com

***Abstract*—In this paper, we employ stochastic geometry to analyze ground-to-unmanned aerial vehicle (UAV) communications. We consider multiple UAVs to provide user-equipments (UEs) with uplink transmissions, where the distribution of UEs follows the Poisson Cluster process (PCP) and each UAV is dedicated to a specific cluster. In particular, we characterize the Laplace transform of the interference caused by multiple UEs in terms of the distribution of UEs as well as the transmission probability of each UE. We then derive analytical expressions of the successful transmission probability. We next conduct a comprehensive numerical analysis with consideration of different system parameters. The results show that four factors (i.e., the geographical surroundings, the transmission powers, the Signal-to-Interference-plus-Noise Ratio (SINR) thresholds, and the UAV height) have main influences on ground-to-UAV communications.**

I. Introduction

UAVs acting as aerial base-stations (BSs) is an emerging solution to flexibly extend the coverage of ground communications. Compared to terrestrial communications with static BSs, the dynamic deployment of UAVs is a more cost-effective solution to on-demand communication requirements [1]. In this context, many related studies have been proposed to explore the optimal deployment scheme of UAVs for improving the relay performance from a ground BS to UEs [2], or maximizing the capacity of covering multiple UEs [3]. In addition, accounting for the practical deployment in a wide region, the performance analysis of UAV-assisted communications is investigated in the previous literature. Particularly, the authors in [4], [5] investigate the communications between UAVs and ground BSs. Furthermore, the authors in [6], [7] employ a stochastic geometry-based model to analyze the transmission performance over the spatial realizations of both UE distributions and UAV deployments. They model the distribution of UEs as Poisson Cluster Process (PCP) for an accurate model where ground nodes are clustered in different areas.

The above-mentioned studies mainly investigate the performance of UAV-to-ground communications from UAVs to UEs [6] or from UAVs to BSs [4]. In contrast, there are few studies [8]–[11] on analyzing the performance of *ground-to-UAV communications* with consideration of UEs' distribution. Nevertheless, ground-to-UAV communications are crucial in practical scenarios, especially for UAV-enabled data collection for UEs (e.g., Internet of Things nodes) [11]. Particularly, they concern different applied scenarios, i.e., UAV-underlay cellular networks [8], one UAV supporting PCP-distributed UEs [9], and two UAVs serving PPP-distributed UEs [10]. In summary, their analytical models focus on the overall coverage performance of a reference UAV under UE's distribution.

However, the end-to-end analytical model related to the particular locations of both the UE and the UAV has not been investigated. To fill this gap, Palm measure can be used to investigate the conditional stochastic distribution of the interference, thereby exploring the transmission performance model for any particular UE-UAV pairs with specific locations. For a UAV located at a certain location, the stochastic characteristics of the cumulative interference depend on the distribution of UEs, with the exclusion of the transmitting UE. Thereafter, we can derive the transmission probability for any particular UE-UAV pair. Moreover, by extending the derived performance model to different transceiver locations, we can further investigate the impact of UAV trajectories on the transmission probability.

The contribution of this paper is firstly investigating the analytical model for any particular UE-UAV transceivers in terms of stochastic distributions of both UEs and UAVs. Specifically, we consider that multiple UAVs are employed to serve UEs. Each UAV is dedicated to one cluster that contains a number of UEs and flies along a certain trajectory to cover its responsible cluster. We formulate the successful probability of a ground-to-UAV transmission for a particular UE-UAV pair based on stochastic geometry. We also conduct numerical results to analyze the successful transmission probability with consideration of multiple system parameters including the UE distributions, the UAV trajectories, the geographical surrounding parameters, and the SINR thresholds. In the rest of this paper, we will first introduce the system model, then analyze stochastic characteristics of the UE's distribution and the interference distribution, next formulate the transmission probability, and finally present numerical results to quantify the impacts of different parameters on the performance.

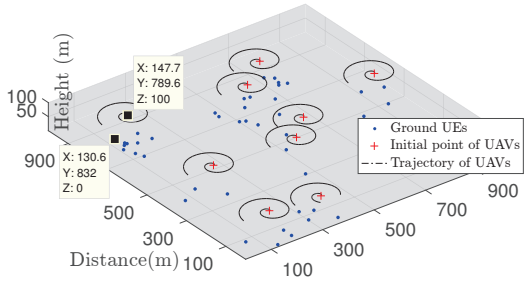

Fig. 1. Illustration of spatial distribution of UAV-enabled communication networks in a 1000m $\times$ 1000m area. The cluster density is 10 clusters/km^2. The mean number of the representative cluster is 5. The radius of each cluster is 100m. Each UAV flies above its served cluster along a spiral trajectory.

II. System Model

A. Network Deployment

We consider a UAV-assisted communication network that multiple UAVs provide a group of UEs with uplink transmission services. As shown in Fig. 1, the UEs follow a clustered distribution in a wide area. Each cluster represents a geographical region containing a number of UEs. One UAV is dispatched to cover a specific cluster as its serving cluster. The total number of the required UAVs depends on the number of the clusters. Each UAV flies along a predefined trajectory to cover all the UEs in its serving cluster. Assume that all UAVs have enough energy to complete their flying as well as communications tasks. Since one UAV is assumed to communicate with only one UE in a time slot, other transmissions from other UEs essentially cause the interference to this UE-to-UAV communication.

We consider that a group of UEs are distributed following a stationary and isotropic PCP denoted by $\Phi_{pcp} = \{x\}$ on the ground, where $x \in \mathbb{R}^2$ denotes the horizontal coordinates of UEs. The center locations of all clusters follow a HPPP denoted by Φ_{hpp}. Assume that all UAVs are located at the same altitude denoted by H_{uav}. The UAVs are dispatched with their initial ground-projection positions distributed as the same HPPP denoted by $\Phi_{hpp} = \{y\}$, where $y \in \mathbb{R}^2$ denotes the ground-projection coordinates of UAVs. Since UAVs fly at the same height, y can uniquely represent the particular location of a UAV. Let $l = \{l(t)\}, l(t) \in \mathbb{R}^2$ denote the trajectory of all UAVs, l includes a series ground-projection traveling points at time slot t in a cluster region, where $t = 0, ..., n, n \in \mathbb{N}$. We assume that all UAVs fly along the same trajectory $l(t)$.

B. Communication Model

1) Path loss models: Let $g(x-y)$ denote the path loss function for the transmitter-receiver pair x, y, where $x - y$ denotes the distance from the UE located at x to the UAV located at y. Referring to the modified LoS/NLoS probability-based path loss model [12], we formulate $g(x-y)$ as follows

$$g(x-y) = g_0 \left(\|x-y\|^2 + H_{UAV}^2 \right)^{\frac{\mathbb{P}_{LOS} \cdot (\varepsilon_{NLoS} - \varepsilon_{LoS}) - \varepsilon_{NLoS}}{2}}, \tag{1}$$

where g_0 is the path loss in a reference distance, given by $(d_0 f_c 4\pi/c)^{-2}$. The term d_0 is the unit distance 1m, f_c is the carrier frequency, and c is the speed of light. The term $\mathbb{P}_{LoS}$ denotes the probability of the LoS path loss, which is given by $1/(1 + \chi \exp(-\xi[\theta - \chi]))$, where χ, ξ are geographical surrounding parameters. The term θ is the UAV elevation angle, given by $180/\pi \arcsin(H_{uav}/d)$, d is the transmission distance given by $\sqrt{\|x-y\|^2 + H_{UAV}^2}$, and ε_{LoS}, ε_{NLoS} are the path loss exponents for the LoS link and the NLoS link, respectively.

2) Transmission possibility: Different UEs may have different transmission possibilities, depending on their practical requirements in a certain time slot. We denote the transmission possibility for the UE located at x by η_x, which is a random variable ranging in $[0, 1]$. The value of η_x represents the transmission probability of the UE located at x initiating a transmission to the UAV.

3) Interference model: When a UE located at x is communicating with the UAV located at y, other simultaneous transmissions from other UEs to the UAV can cause the interference. Assume that all UEs have the same transmission power denoted by p. The interference to a specific communication is modelled as a shot-noise process [13] as follows

$$I_\Phi(y) = \sum_{x \in \Phi_{pcp}} \eta_x p h g(x-y), \tag{2}$$

where h is the channel fading coefficient for the small-scale fading. We consider the small-scale fading channel to demonstrate the time-variant property of the ground-to-UAV channel in the case of the low altitude (lower than 100m) communications of UAVs [14]. The amplitude fading $\sqrt{h}$ is assumed to follow Rayleigh fading, and then the powers h are exponentially distributed with the mean μ. We assume that h is randomly distributed with the time and also independent of the distribution of the transmitter-receiver pair.

4) SINR model: For a certain communication initiated from a particular UE located at $x' \in \phi_y$, the received power of a UAV located at y is modeled as $phg(x'-y)$. Let W denote the Additive White Gaussian Noise in communications. The Signal-to-Interference-plus-Noise Ratio (SINR) is given by

$$\gamma(x', y) = \frac{phg(x'-y)}{W + I_{\phi \setminus \{x'\}}(y)}. \tag{3}$$

We observe that the value of $I_\Phi(y)$ depends on the locations of y while the value of $\gamma(x', y)$ depends on both the locations of x' and y. The communication from a UE located at x ($x \in \phi_y$) to a UAV located at y is successful if and only if the SINR is beyond the threshold value γ_0, i.e., $\gamma(x, y) \geq \gamma_0$.

III. Stochastic Characteristic

A. Spatial Characteristics

We model Φ_{pcp} as a Neyman-Scott cluster process. Neyman-Scott cluster process is a special PCP with stationary and isotropic properties. Let $\Phi_{pcp} = \bigcup_{y \in \Phi_{hpp}} \phi_y$, where y denotes the parent points following $\Phi_{hpp} = \{y\}$ with intensity λ_p. The clusters are in the form $\phi_y = \phi + y$ for each y, where ϕ denotes a group of i.i.d. finite daughter points with

distribution independent of the parent process. Let ϕ_0 denote the representative cluster that is constituted by independently scattered daughter points with identical distribution $F(A) = \int_A f(x)\mathrm{d}x, A \subset \mathbb{R}^2$ around the center of this cluster. The intensity of the complete process Φ is $\lambda = \lambda_p \bar{c}$ with $\bar{c}$ being the average number of points in the representative cluster ϕ_0.

To ensure the isotropic scattering of the daughter process, we use a classic clustering model namely Matern cluster processes (MCP) [15]. For the cluster of MCP, each point is uniformly distributed in a circle of radius a around the origin. The density function of MCP is given by

$$f(x) = \frac{1}{\pi a^2}, \|x\|^2 \leq a. \tag{4}$$

Let $v(x)$ is any integrable and non-negative functions. The probability generating functional $G_p\left(v(x)\right) = \mathbb{E}\left(\prod_{x\in\Phi_{pcp}} v(x)\right)$ of the Neyman-Scott cluster process Φ_{pcp} is given by [15], [16] as follows

$$G_p\left(v(x)\right) = \exp\left(-\lambda_p \int_{\mathbb{R}^2} \left[1 - G_k\left(v(x)\right)\right] \mathrm{d}k\right), \tag{5}$$

where $G_k\left(v(x)\right) = M\left(\int_{\mathbb{R}^2} v(x+k) f(x)\mathrm{d}x\right)$ is the probability generating functional of the cluster with its center located at k, $M(\cdot)$ is the moment generating function of the number of points in the representative cluster. It is worth noting that the dot '$\cdot$' represents the variable, on which the function is acting. We then use '$\cdot$' to describe variables in the other functions in the rest of this paper. In the case of MCP, the mean number of points in representative cluster is $\bar{c}$, $M(\cdot) = \exp(-\bar{c}(1-\cdot))$.

In addition, the probability generating functional $G_0\left(v(x)\right)$ of the representative cluster ϕ_0 of a Neyman-Scott cluster process is given by [15], [16] as follows

$$G_0\left(v(x)\right) = M\left(\int_{\mathbb{R}^2} v(x) f(x)\mathrm{d}x\right). \tag{6}$$

We use the combined super/sub-script $^{!}_{x'}$ represents a series of conditional measure given that a point is located at x'. Herein, the superscript $^{!}$ denote a stochastic function with respect to the reduced Palm measure [15]. It basically denotes the conditional measure with the conditioning on a point is observed at a certain location. The subscript $_{x'}$ denotes the coordinates of the certain location in the reduced Palm measure. For example, $\mathbb{P}^{!}_{x'}(\cdot)$ denotes the conditional distribution probability that is essentially the conditional probability of point process events with the conditioning on a point at x'.

We then present Lemma 1 to derive the conditional probability generating functional of Φ_{pcp} when a point is located at x'.

Lemma 1. *Let $G^{!}_{x'}\left(v(x)\right) = \mathbb{E}^{!}_{x}\left(\prod_{x\in\Phi_{pcp}} v(x)\right)$ be the conditional generating functional of the Neyman-Scott cluster process Φ_{pcp} with the conditioning on a point located at x'. Then $G^{!}_{x'}\left(v(x)\right)$ can be calculated by*

$$G^{!}_{x'}\left(v(x)\right) = \theta_1 \exp\left(-\theta_2(x')\right), \tag{7}$$

where $\theta_1 = \exp\left(-\lambda_p \int_{\mathbb{R}^2} 1 - \exp\left(-\theta_2(k)\right)\mathrm{d}k\right)$, $\theta_2(k) = \bar{c}\int_{\mathbb{R}^2}(1 - v(x+k)) f(x)\mathrm{d}x$, and $\theta_2(x') = \theta_2(k)|_{k=x'}$.

Proof: The detailed proof is given in Appendix A. ■

We observe that given two functions $v(\cdot)$ and $f(\cdot)$, $G^{!}_{x'}\left(v(x)\right)$ is independent of the location x'.

B. Laplace Transform of the Interference

We next analyze the interference when the UE located at x' is communicating with the UAV located at y, where x' can be an arbitrary point in the Neyman-Scott cluster process Φ_{pcp}, and y is the location of the dedicated UAV for the cluster including point x'.

Lemma 2. *The conditional Laplace transform of the interference for a UE located at x' and the UAV located at y is given by*

$$\mathcal{L}_{I_{\Phi/x'}(y)}(s) = G^{!}_{x'}\left(\frac{\mu}{\mu + s\eta_x p g(x-y)}\right). \tag{8}$$

Proof: The detailed proof is given in Appendix B. ■

Proposition 1. *Substituting the formulation of $G^{!}_{x'}(\cdot)$ in Eq. (7) to Lemma 2, we have*

$$\mathcal{L}_{I_{\Phi/x'}(y)}(s) = \vartheta_1(s,y)\exp\left(-\vartheta_2(s,x',y)\right), \tag{9}$$

where $\vartheta_1(s,y) = \exp\left(-\lambda_p \int_{\mathbb{R}^2} 1 - \exp\left(-\vartheta_2(s,k,y)\right)\mathrm{d}k\right)$, $\vartheta_2(s,k,y) = \bar{c}\int_{\mathbb{R}^2} \frac{f(x)}{1+\frac{\mu}{s\eta_{x+k} p g(x+k-y)}}\mathrm{d}x$ and $\vartheta_2(s,x',y) = \theta_2(k,y)|_{k=x'}$.

It is observed that the conditional Laplace transform of the interference $\mathcal{L}_{I_{\Phi/x'}(y)}(s)$ depends on both positions of a given UE located at x' and its responsible UAV located at y. This implies that $I_\Phi(y)$ is a non-stationary stochastic process.

IV. Communication Performance Analysis

A. Successful Transmission Formulation

The successful transmission depends on the value of SINR, with the condition that SINR at the receiver is higher than the threshold of SINR. For the communication link that is established from a typical UE located at x' to the UAV located at y', the transmission is successful when its SINR is higher than the threshold value, i.e., $\gamma(x',y) \geq \gamma_0$.

Theorem 1. *The transmission probability for a particular communication link that connects the UE located at x' to the UAV located at y is given by*

$$\mathbb{P}_{suc}\left(x',y\right) = \exp\left(-\frac{\mu\gamma_0 W}{p g(x'-y)}\right)\varrho_1(y)\exp\left(-\varrho_2(x',y)\right), \tag{10}$$

where $\varrho_1(y) = \exp\left(-\lambda_p \int_{\mathbb{R}^2} 1 - \exp\left(-\varrho_2(k,y)\right)\mathrm{d}k\right)$, $\varrho_2(k,y) = \bar{c}\int_{\mathbb{R}^2} \frac{f(x)}{1+\frac{g(x'-y)}{\gamma_0 \eta_{x+k} g(x+k-y)}}\mathrm{d}x$ and $\varrho_2(x',y) = \theta_2(k,y)|_{k=x'}$.

Proof: The detailed proof is given in Appendix C. ■

Remark 1. Theorem 1 shows the complete formulation of the successful transmission probability $\mathbb{P}_{suc}(x',y)$ of a particular communication link from the UE x' to the UAV y. Explicitly, the value of $\mathbb{P}_{suc}(x',y)$ is not only determined by the particular locations of x' and y but also related to some

system parameters, i.e., the mean value μ of the small-scale fading amplitude, the noise power W, the cluster density λ_p, the mean number $\bar{c}$ of points in the representative cluster, γ, and the transmission power p). It is also influenced by three functions, i.e., η_x, $f(x)$, $g(x)$. Obviously, μ, W, p, and λ_p have linear relationships with $\mathbb{P}_{suc}(x', y)$. Other impact factors have different non-linear influences on $\mathbb{P}_{suc}(x', y)$.

Remark 2. Note that the ground-to-UAV path loss model significantly affects the transmission probability $\mathbb{P}_{suc}(x', y)$. As in Eq. (1), $g(\cdot)$ is determined by two factors: the LoS probability $\mathbb{P}_{LoS}$ and the communication distance. The value of $\mathbb{P}_{LoS}$ is mainly determined by the geographical surrounding factors χ and ξ, which are associated with the building density and height, etc. For this reason, we can find a relationship between the value of $\mathbb{P}_{suc}(x', y)$ and the geographical surrounding parameters.

Remark 3. Except for the geographical surroundings, three basic system parameters, the transmission power p, the SINR threshold γ_0, and the distance $\|x - y\|$, are crucial for ground-to-UAV communications. A larger value of p or a smaller value of γ_0 indicates a stronger adaptability for deteriorated channel fading and a longer transmission distance also implies a higher transmission probability. Hence, the value of p and γ_0 determine the available range of the transmission distance. In the contrast, a longer transmission distance or a higher altitude of the UAV may lead to a lower transmission probability.

B. Numerical Analysis

We next conduct a comprehensive numerical analysis on the transmission probability against different system parameters. We select particular coordinates x', y of the UE and the UAV, respectively. We consider a 1000m $\times$ 1000m region, where 1000 is chosen as the integration upper limit. To ensure the available value of $f(x)$, the integration in ϱ_2 is transformed to a polar-coordinate system by setting the cluster radius as 100m. The path loss exponents of LoS and NLoS are chosen as $\varepsilon_{LoS} = 2.1, \varepsilon_{NLoS} = 2.4$, respectively [17]. The carrier frequency $f_c = 2.4$GHz and the noise power $W = 10^{-12}$W.

1) The Geographical Distribution: In Fig. 2, we plot the transmission probability $\mathbb{P}_{suc}(x', y)$ against different geographical distributions. We set $y = (195, 195)$ and $x' = (100, 100)$, for a case that the UAV locates a cluster center $(195, 195)$ with radius 100m and the UE locates the edge of this cluster. In addition, the geographical surrounding factors χ, ξ are set to be $4.88, 0.429$ for suburban, $9.617, 0.1581$ for urban, $12.081, 0.1139$ for dense urban, and $27.2304, 0.0797$ for highrise urban respectively [18]. The transmission power $p = 0.1$W, the SINR threshold $\gamma_0 = -15$dB, and the UAV height $H_{uav} = 30$m.

As shown in Fig. 2a, different geographical surroundings have significant influences on the transmission probability. Specifically, a suburban environment obtains a much higher transmission probability than urban or dense urban environment. With sparse and low obstacles on the ground, the suburban area has a higher LoS probability than the urban area with dense and high buildings. Consequently, the suburban

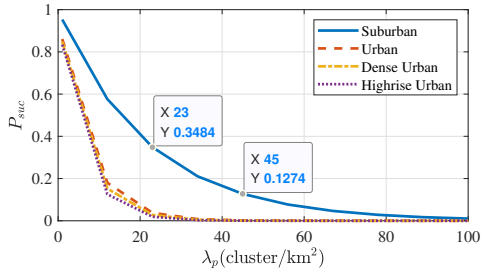

(a) $\bar{c} = 5$

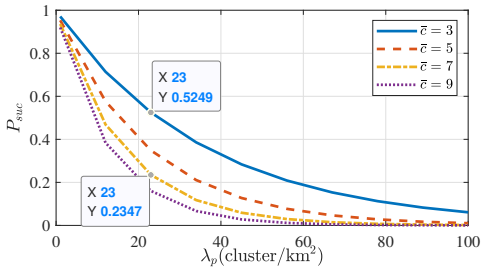

(b) Surburban

Fig. 2. The communication probability against the cluster density λ_p in different geographical surroundings and different mean numbers $\bar{c}$ of points in the representative cluster.

area gets a better propagation condition, thereby achieving a higher transmission probability than the urban area.

In addition, the distribution of UEs has significant impact on the transmission probability. As shown in Fig. 2, $\mathbb{P}_{suc}(x', y)$ decreases exponentially with the cluster density λ_p being linearly increased from 1 cluster/km^2 to 100 clusters/km^2. Meanwhile, the transmission performance drops with the increasing mean numbers (from $3 - 9$) in the representative cluster $\bar{c}$ as shown in Fig. 2b.

2) The UAV height and the SINR threshold: In Fig. 3, we plot the transmission probability $\mathbb{P}_{suc}(x', y)$ against the UAV height H_{uav} and the SINR threshold γ_0 for different transmission powers p. We also set $y = (195, 195)$ and $x' = (100, 100)$ as the same as that in Fig. 2. The surrounding parameters are chosen as suburban environment, i.e., $\chi = 4.88$, $\xi = 0.429$. The UE distribution has fixed parameters that $\lambda_p = 5$ cluster/km^2, $\bar{c} = 5$.

Fig. 3a shows that the value of $\mathbb{P}_{suc}(x', y)$ first increases and then turns to a stable trend with the increment of H_{uav}. At the beginning when H_{uav} is increased, the decreased interference dominates the transmission performance, thereby improving the transmission probability. Then, when the UAV height exceeds a value (about 30m when $x' = (100, 100)$), the deteriorated power fading effect dominates the transmission performance, consequently leading to the decreased transmission probability. Notably, the curve is sensitive to the UE's location. When changing the UE's location to $x' = (150, 150)$ or $x' = (200, 200)$, the UE is clearly closer to the UAV, thus the interference's impact is nearly getting neglect. Specifically, in the case of $x' = (200, 200)$, we get a flat curve with only

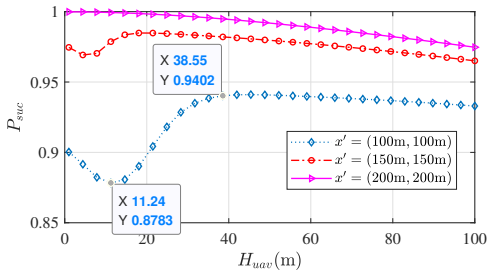

(a) $\gamma_0 = -15\text{dB}, p = 0.1\text{W}$

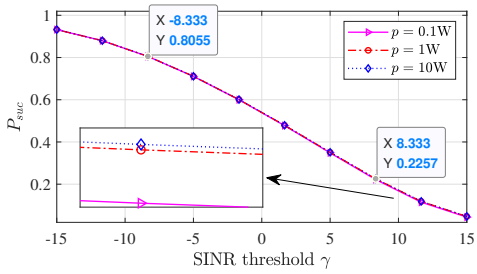

(b) $H_{uav} = 30\text{m}, x' = (100, 100)$

Fig. 3. The communication probability against the UAV height H_{uav} and the SINR threshold γ_0 for different transmission powers p of ground UEs.

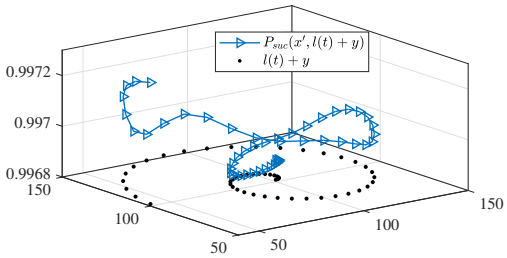

(a) Spiral Trajectory

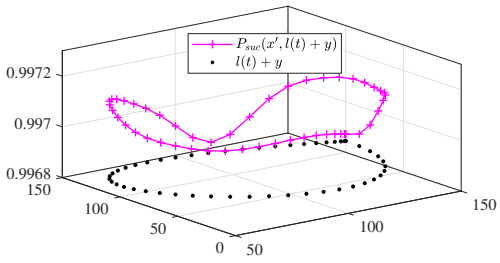

(b) Circular Trajectory

Fig. 4. The communication probability against the UAV's traveling points in two trajectories (spiral trajectory and circular trajectory).

the slowly dropping trend against the increasing height of the UAV.

Additionally, we can observe from Fig. 3b that the value of $\mathbb{P}_{suc}(x', y)$ significantly decreases with the increased SINR threshold. Certainly, the smaller SINR threshold in the receiver indicates a sharp receiving condition, thus resulting in a lower transmission probability. In contrast, the changing transmitter power has much slighter impact on the transmission probability. With the increasing transmission power (i.e., $0.1\text{W}, 1\text{W}, 10\text{W}$),the transmission probability has very slight increment. Imperatively, the larger transmission power or the smaller value of the SINR threshold indicates stronger adaptability for deteriorated channel fading and longer transmission distance, implying higher transmission probability.

3) The UAV Trajectory: Fig. 4 plots the transmission probability $\mathbb{P}_{suc}(x', y)$ against two different UAV trajectories (spiral trajectory and circular trajectory). The spiral trajectory is modelled by

$$l(t) = \left(\frac{10t}{\pi}\cos\left(\frac{t}{2}\right), \frac{10t}{\pi}\sin\left(\frac{t}{2}\right)\right), t \in (0, 6\pi).$$

The circular trajectory is modelled by

$$l(t) = (66 \cdot \cos(t), 66 \cdot \sin(t)), t \in (0, 2\pi).$$

Both two trajectories are generated around a cluster center at $(100, 100)$. We consider 50 traveling points $y = l(t) + (100, 100)$ for each trajectory and the associated UE is set to be a neighbor location $x = y - (5, 5)$. Furthermore, we set the system parameters as follow: $p = 0.1\text{W}, \gamma_0 = -15\text{dB}, H_{uav} = 30\text{m}, \lambda_p = 5\ \text{clusters/km}^2, \bar{c} = 5$ in a suburban area.

Fig. 4 depicts the transmission probabilities against the traveling points in two trajectories. We observe that $\mathbb{P}_{suc}(x', y)$ varies with different traveling points of y though the average variance of transmission probability is very small (about 0.0001) for both two trajectories. This phenomenon can be explained by the fact that the random disturbance is caused by the randomly-generated transmission possibilities when the UAV flies along with different traveling points. Clearly, this time-variance has a quite little impact on the transmission compared with other system parameters as aforementioned.

In summary, the transmission possibility for a particular ground-to-UAV communication link is mainly impacted by four system parameters, i.e., the geographical surrounding factors, the density of UEs, the SINR threshold, and the UAV height. The transmission probability is also influenced by the transmission power and the trajectory of the UAV though their impacts are much smaller than the aforementioned four system parameters.

V. Conclusion

This paper presents a stochastic geometry-based performance analysis for ground-to-UAV communications. In particular, we establish a model to analyze the successful transmission probability by considering stochastic characteristics of interference caused by PCP-distributed UEs. We conduct the comprehensive numerical analysis with consideration of multiple system parameters, including geographical surroundings, the UAV heights, SINR thresholds, and cluster densities. In future research, we will consider the introduction of remote ground base-stations and also analyze more communication performance metrics (such as spectrum efficiency and network

coverage).

APPENDIX A

Proof of Lemma 1: Let $\mathbb{P}$ be the distribution of the PCP Φ_{pcp} and $\boldsymbol{c}_{x'}$ be the conditional distribution of the cluster $\phi_{x'}$ conditioning on a point at the location x'. The conditional distribution of a point at x' of Φ_{pcp} is then given by $\mathbb{P}^!_{x'} = \mathbb{P} * \boldsymbol{c}^!_{x'}$ [15], where $*$ denotes the convolution of two distributions. According to Campbell theorem, we can calculate $G^!_{x'}(v(x))$ as follows

$$\begin{aligned} G^!_{x'}(v(x)) &= \mathbb{E}^!_x\left(\prod_{x\in\Phi_{pcp}} v(x)\right) = \int_{\mathbb{R}^2}\prod_{x\in\Phi_{pcp}} v(x)\mathbb{P}^!_{x'}(\mathrm{d}\Phi_{pcp}) \\ &= \int_{\mathbb{R}^2}\prod_{x\in\Phi_{pcp}} v(x)\int_{\mathcal{N}}\mathbb{P}\left(\mathrm{d}\left(\Phi_{pcp}-\psi\right)\right)\boldsymbol{c}^!_{x'}(\mathrm{d}\psi) \\ &= \int_{\mathbb{R}^2}\prod_{x\in\Phi_{pcp}} v(x)\mathbb{P}(\mathrm{d}\Phi_{pcp})\int_{\mathcal{N}}\prod_{x\in\psi} v(x)\boldsymbol{c}^!_{x'}(\mathrm{d}\psi) \\ &= G_p\left(v(x)\right)G_0\left(v(x+x')\right), \end{aligned}$$

where $G_p(v(\cdot))$ is the generating functional of Φ_{pcp} and $G_0(v(\cdot))$ is the generating functional of ϕ_0. Substituting the expressions of $G_p(v(\cdot))$ and $G_0(v(\cdot))$ in Eq. (5) and Eq. (6), we have the result in Lemma 1. ■

APPENDIX B

Proof of Lemma 2: Let $\mathcal{L}_h(\cdot)$ denote the Laplace transform of the fading random variable h. We then have

$$\begin{aligned} \mathcal{L}_{I_{\Phi/x'}(y)}(s) &= \mathbb{E}^!_{x'}\left[\exp\left(-s\sum_{x\in\Phi_{pcp}}\eta_x phg(x-y)\right)\right] \qquad (11) \\ &= \mathbb{E}^!_{x'}\left[\prod_{x\in\Phi_{pcp}}\exp\left(-s\eta_x phg(x-y)\right)\right] \\ &\overset{(a)}{=} \mathbb{E}^!_{x'}\left[\prod_{x\in\Phi_{pcp}}\mathcal{L}_h\left(s\eta_x pg(x-y)\right)\right] \\ &\overset{(b)}{=} G^!_{x'}\left(\mathcal{L}_h\left(s\eta_x pg(x-y)\right)\right), \end{aligned}$$

where (a) follows from the independence of h, and (b) comes from the conditional generating functional of Φ_{pcp} as shown in Eq. (7), h is exponentially distributed with mean μ, then $\mathcal{L}_h(\cdot) = \int_0^\infty \mu\exp(-\mu h)\exp(-\,\cdot\, h)\mathrm{d}h = \mu/(\cdot+\mu)$, thus leading to the result. ■

APPENDIX C

Proof of Theorem 1: We have

$$\begin{aligned} \mathbb{P}_{suc}\left(x',y\right) &= \mathbb{P}\left(\gamma(x',y)\geq\gamma_0\right) \\ &\overset{(a)}{=} \mathbb{E}^!_{x'}\left(\exp\left(-\frac{\mu\gamma_0\left(W+I_\Phi(y)\right)}{pg(x'-y)}\right)\right) \\ &= \exp\left(-\frac{\mu\gamma_0 W}{pg(x'-y)}\right) \\ &\quad\times\mathbb{E}^!_{x'}\left(\exp\left(-\frac{\mu\gamma_0}{pg(x'-y)}I_\Phi(y)\right)\right) \\ &\overset{(b)}{=} \exp\left(-\frac{\mu\gamma_0 W}{pg(x'-y)}\right)\mathcal{L}_{I_{\Phi/x'(y)}}\left(-\frac{\mu\gamma_0}{pg(x'-y)}\right), \end{aligned}$$

where (a) follows the distribution function of h, i.e., $\mathbb{P}(h\geq h') = \exp(-\mu h')$ due to h being exponentially distributed with mean μ, (b) follows the definition of conditional Laplace transform of the interference $I_\Phi(y)$. Obviously, the $\mathbb{P}_{suc}(x',y)$ can be further evaluated by substituting the formulation of the conditional Laplace transform of the interference $\mathcal{L}_{I_{\Phi/x'}(y)}(\cdot)$. Substituting Proposition 1 to the above equation, we have the result. ■

ACKNOWLEDGMENT

This paper was partially supported by Macao Science and Technology Development Fund under Grant No. 0026/2018/A1.

REFERENCES

[1] Y. Zeng, Q. Wu, and R. Zhang, "Accessing from the sky: A tutorial on UAV communications for 5G and beyond," *Proceedings of the IEEE*, vol. 107, no. 12, pp. 2327–2375, 2019.

[2] A. Fotouhi, M. Ding, L. Galati Giordano, M. Hassan, J. Li, and Z. Lin, "Joint Optimization of Access and Backhaul Links for UAVs Based on Reinforcement Learning," in *2019 IEEE Globecom Workshops (GC Wkshps)*, 2019, pp. 1–6.

[3] T. M. Nguyen, W. Ajib, and C. Assi, "A Novel Cooperative NOMA for Designing UAV-Assisted Wireless Backhaul Networks," *IEEE Journal on Selected Areas in Communications*, vol. 36, no. 11, pp. 2497–2507, 2018.

[4] B. Galkin, J. Kibilda, and L. A. DaSilva, "Backhaul for Low-Altitude UAVs in Urban Environments," in *2018 IEEE International Conference on Communications (ICC)*, 2018, pp. 1–6.

[5] M. Gapeyenko, V. Petrov, D. Moltchanov, S. Andreev, N. Himayat, and Y. Koucheryavy, "Flexible and Reliable UAV-Assisted Backhaul Operation in 5G mmWave Cellular Networks," *IEEE Journal on Selected Areas in Communications*, vol. 36, no. 11, pp. 2486–2496, 2018.

[6] B. Galkin, J. Kibiłda, and L. A. DaSilva, "A Stochastic Model for UAV Networks Positioned Above Demand Hotspots in Urban Environments," *IEEE Transactions on Vehicular Technology*, vol. 68, no. 7, pp. 6985–6996, 2019.

[7] W. Yi, Y. Liu, Y. Deng, and A. Nallanathan, "Clustered UAV Networks with Millimeter Wave Communications: A Stochastic Geometry View," *IEEE Transactions on Communications*, 2020.

[8] X. Zhou, J. Guo, S. Durrani, and H. Yanikomeroglu, "Uplink Coverage Performance of an Underlay Drone Cell for Temporary Events," in *2018 IEEE International Conference on Communications Workshops (ICC Workshops)*, 2018, pp. 1–6.

[9] W. Yi, Y. Liu, A. Nallanathan, and G. K. Karagiannidis, "A Unified Spatial Framework for Clustered UAV Networks Based on Stochastic Geometry," in *2018 IEEE Global Communications Conference (GLOBECOM)*, 2018, pp. 1–6.

[10] J. Li, Y. Liu, X. Li, C. Shen, and Y. Chen, "Non-Orthogonal Multiple Access in Cooperative UAV Networks: A Stochastic Geometry Model," in *2019 IEEE 90th Vehicular Technology Conference (VTC2019-Fall)*, 2019, pp. 1–6.

[11] T. Shafique, H. Tabassum, and E. Hossain, "End-to-End Energy-Efficiency and Reliability of UAV-Assisted Wireless Data Ferrying," *IEEE Transactions on Communications*, vol. 68, no. 3, pp. 1822–1837, 2020.

[12] Y. Liu, H.-N. Dai, H. Wang, M. Imran, X. Wang, and M. Shoaib, "UAV-enabled data acquisition scheme with directional wireless energy transfer for Internet of Things," *Computer Communications*, 2020.

[13] R. K. Ganti and M. Haenggi, "Interference and Outage in Clustered Wireless Ad Hoc Networks," *IEEE Transactions on Information Theory*, vol. 55, no. 9, pp. 4067–4086, 2009.

[14] W. Khawaja, I. Guvenc, D. W. Matolak, U.-C. Fiebig, and N. Schneckenburger, "A survey of air-to-ground propagation channel modeling for unmanned aerial vehicles," *IEEE Communications Surveys & Tutorials*, vol. 21, no. 3, pp. 2361–2391, 2019.

[15] S. N. Chiu, D. Stoyan, W. S. Kendall, and J. Mecke, *Stochastic geometry and its applications*. John Wiley & Sons, 2013.

[16] D. R. Cox and V. Isham, *Point processes*. CRC Press, 1980, vol. 12.

[17] M. Chen, M. Mozaffari, W. Saad, C. Yin, M. Debbah, and C. S. Hong, "Caching in the sky: Proactive deployment of cache-enabled unmanned aerial vehicles for optimized quality-of-experience," *IEEE Journal on Selected Areas in Communications*, vol. 35, no. 5, pp. 1046–1061, 2017.

[18] A. Al-Hourani, S. Kandeepan, and S. Lardner, "Optimal LAP altitude for maximum coverage," *IEEE Wireless Communications Letters*, vol. 3, no. 6, pp. 569–572, 2014.